The current issue and full text archive of this journal is available at
www.emeraldinsight.com/0961-5539.htm

Entropy generation due to jet impingement on a surface: effect of annular nozzle outer angle

S.Z. Shuja, B.S. Yilbas and M.O. Budair
ME Department, KFUPM, Dhahran, Saudi Arabia

Received 12 June 2006
Revised 10 October 2006
Accepted 16 November 2006

Abstract

Purpose – The purpose of this paper is to examine entropy generation rate in the flow field due jet emanating from an annular nozzle and impinging on to a flat plate. Since the flow field changes with the geometric configuration of the annular nozzle, the influence of nozzle outer cone angle on the entropy generation rate is considered.

Design/methodology/approach – The steady flow field pertinent to jet impingement on to a flat plate is modeled with appropriate boundary conditions. A control volume approach is introduced to discretize the governing equations of flow and to simulate the physical situation numerically. Entropy generation rate due to heat transfer and fluid friction is formulated. The resulting entropy equations are solved numerically.

Findings – Thermodynamic irreversibility, which is quantified through entropy generation rate, gives insight into the thermodynamics losses in the flow system. Entropy generation rate is highly affected by the nozzle outer cone angle. In this case, increasing nozzle outer cone angle enhances the entropy generation rate, particularly due to fluid friction.

Research limitations/implications – The predictions may be extended to include the nozzle area ratio and mass flow rate variation.

Practical implications – The paper is a very useful source of physical information for improving nozzle design, particularly that which is used in a laser thick material cutting operation. It disseminates information for those working on both laser machining applications and entropy generation in flow systems.

Originality/value – This paper discusses the physical issues related to the entropy generation rate and offers practical help to an individual starting out on an academic career.

Keywords Thermodynamic properties, Fluid phenomena, Jets, Substrates

Paper type Research paper

Nomenclature

D = nozzle exit diameter (m)
H = enthalpy
K = thermal conductivity
k = turbulent kinetic energy
K_{eff} = effective thermal conductivity (W/mK)
K_{l} = bulk thermal conductivity (W/mK)
K_{t} = turbulent thermal conductivity (W/mK)
p = pressure
P = rate of production
R_{ij} = Reynolds stress
Re = Reynolds No.
r = distance in the radial direction
$\dot{S}'''_{\text{gen}}$ = volumetric entropy generation rate (W/m^{3}K)
t = time

The authors acknowledge the support of King Fahd University of Petroleum and Minerals, Dhahran, Saudi Arabia, for this work.

International Journal of Numerical Methods for Heat & Fluid Flow
Vol. 17 No. 7, 2007
pp. 677-691

0961-5539
DOI 10.1108/09615530710777958

T = temperature
u^* = friction velocity
U = arbitrary velocity
V = axial velocity component
W = radial velocity component
$\forall$ = volume
z = distance in the axial direction

Greek

α = thermal diffusivity
Γ = arbitrary diffusion coefficient
ε = energy dissipation
λ = turbulence intensity
μ_{eff} = effective viscosity (Ns/m^2)
μ_t = turbulent viscosity (Ns/m)
μ_l = laminar viscosity (Ns/m^2)
ν = kinematic viscosity
ρ = density (function of temperature and pressure for gas)
σ = variable Prandtl No.
θ = nozzle cone angle

Φ = viscous dissipation
ϕ = arbitrary variable
Π = energy transport due to pressure excluding strain interactions
Π^{w} = energy transport due to wall reflection
Λ = energy transport by diffusion

Subscript

amb = ambient
i, j = arbitrary direction
jet = gas jet at inlet
l = laminar
max = maximum
p = a typical node in the computational grid
t = turbulent
v = viscous sub-layer
w = wall
v = viscous sublayer

1. Introduction

Annular nozzles can be used to improve laser deep penetrated processing of metallic substrates. In this case, gas emerging from the nozzle impinges onto the surface of the workpiece. Flow structure around the surface of the workpiece influences significantly heat transfer rates from the surface. Moreover, flow structure in this region is influenced by the nozzle geometric configurations. Thermodynamic irreversibility associated with flow field gives insight into the flow structure of the impinging jet. Entropy generation in the flow system provides information in thermodynamic irreversibility. Consequently, investigation into entropy generation during jet emerging from annular nozzle and impinging onto a flat plate surface becomes essential.

Considerable research studies were carried out to examine jet impingement onto surfaces. The effect of nozzle diameter on heat transfer characteristics from the impinging surface was studied by Lee *et al.* (1995). They showed that local Nusselt number increased with increasing jet diameter in the stagnation region, which was attributed to an increase in the jet momentum and turbulence intensity level with the large nozzle diameter. Effect of nozzle geometry on flow characteristics and heat transfer from impinging surfaces was examined by Dano (2005). They indicated that the flow development from the cusped ellipse nozzle affected the wall region flow more than the circular nozzle; in addition, the overall heat transfer for the uniform heat flux boundary condition was found to increase when the cusped ellipse nozzle was used. The effects of nozzle configuration on cooling rates from concave surfaces were investigated by Yang *et al.* (1999). They showed that average heat transfer rates for impingement on the concave surface was more than the flat plate. Heat transfer rates from impinging surface due to annular jet were studied by Hiroshi and Akira (1989). They showed that the flow pattern of the annular impinging jet was divided in three regions and that the Nusselt number in the stagnation region had a weak dependency

on the Reynolds number. The effect of nozzle geometry on local convective heat transfer due to a confined impinging air jet was investigated by Colucci and Viskanta (1996). They indicated that the local heat transfer coefficients for confined jet were more sensitive to Reynolds numbers and nozzle-to-plate spacing than those for unconfined jets. Jet impingement and heat transfer due to low nozzle-plate spacing was examined by Lytle and Webb (1994). They showed that the outer peak in local Nusselt number was found to move radially outward for large nozzle-to-plate spacings and higher jet Reynolds numbers. Heat transfer due to an impinging jet on a flat plate was studied by Huang and El-Genk (1994). They showed that maximum Nusselt number was strong function of nozzle-to-plate spacing and nozzle diameter. Heat transfer from impinging surface due to a round jet was examined by Mohanty and Tawfek (1993). They introduced functional relation between the nozzle effective area and heat transfer rates from the surface. The influence of nozzle geometric configurations on flow structure and heat transfer rates in the stagnation region were examined by Shuja *et al.* (2005). They showed that nozzle configuration had significant effect on the heat transfer rates from the flat surface and complex flow structure was formed in the stagnation region. However, thermodynamic analysis for irreversibility in the flow system was left obscure.

Thermodynamic irreversibility analysis provides process optimization and improved design configurations of thermal systems (Bejan, 1982). The rate of entropy generation can be used to quantify thermodynamic irreversibility in the flow system. Considerable research studies were carried out to examine entropy generation in flow systems. Entropy generation and minimization in thermal systems for improved operation and design was examined by Bejan (1982). He showed that entropy generation rate could be used as an effective tool for optimum design of thermal systems. The second law analysis in convective heat transfer problems was investigated by Mahmud and Eraser (2003). They developed an analytical expression for Bejan number due to different flow situations. Entropy generation in developing and fully developed flows was studied by Carrington and Sun (1992). They formulated entropy production rate in terms of flow properties. Second law analysis in swirling flow was carried out by Mukherjee *et al.* (1987). They determined local Nusselt number and rate of entropy production. Entropy generation in pipe flow due to restrictions was examined by Yilbas *et al.* (1999). They developed relation between entropy production rate, Swirl and Merit numbers.

In the present study, entropy generation in the flow system due to jet emerging from an annular nozzle and impinging onto a flat plate is considered. Effect of nozzle geometric con-figurations on entropy generation rate is examined. A numerical scheme employing a control volume approach is introduced in the simulations and air is used as impinging gas.

2. Flow analysis

In laser gas assisted processing, the impinging jet conditions are mainly steady; consequently, a steady flow conditions are considered in the analysis, provided that the compressibility effect and variable properties are accommodated. The jet impinging onto a uniformly heated flat plate is simulated. The heat source with a constant heat flux is considered at the plate surface. The geometric arrangements of the annular

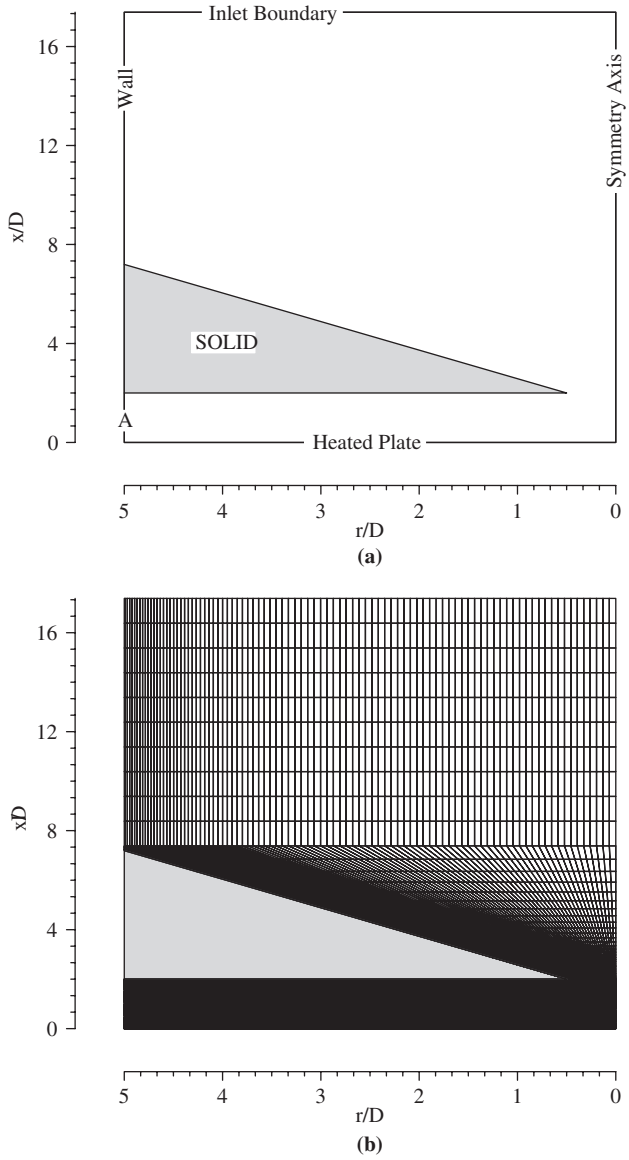

Figure 1.
Cross-sectional view of conical nozzle: (a) boundary conditions; and (b) grid used in the simulations. The cone angle of the nozzle is 25°

Nozzle No.	Cone angle (θ°)
1	25
2	35
3	45
4	55

Table I.
Geometry configuration of annular conical nozzle

conical nozzle is shown in Figure 1(a) while the nozzle outer cone angles are given in Table I. It should be noted that the nozzle inner angle is kept constant at 20°.

2.1 Flow equations

The flow equations for the axisymmetric impinging jet can be written as: the continuity equation yields:

$$\frac{\partial}{\partial x_i}(\rho U_i) = 0 \tag{1}$$

The momentum equation yields:

$$\frac{\partial}{\partial x_i}(\rho U_i U_j) = -\frac{\partial p}{\partial x_j} + \frac{\partial}{\partial x_i}\left[\mu\left(\frac{\partial U_i}{\partial x_j} + \frac{\partial U_j}{\partial x_i}\right) - \rho R_{ij}\right] \tag{2}$$

The energy equation yields:

$$\frac{\partial}{\partial x_i}(\rho U_i H) = \frac{\partial}{\partial x_i}\left[\frac{\mu}{\sigma}\frac{\partial H}{\partial x_i} - \rho R_{ih}\right] \tag{3}$$

The following steps are considered to determine the Reynolds stresses and turbulence properties.

2.1.1 Reynolds stresses (R_{ij}). The Reynolds stress turbulence model (RSTM) is based on the second-moment closure (Launder, 1989). The transport equation of the Reynolds stress (R_{ij}) is:

$$\frac{\partial}{\partial x_m}(U_m R_{ij}) = P_{ij} + \Lambda_{ij} - \varepsilon_{ij} + \Pi_{ij} + \Pi_{ij}^{w} \tag{4}$$

where P, Λ ε, $\int$ and $\int^{w}$ are the rate of production, transport by diffusion, rate of dissipation, transport due to turbulent pressure excluding strain interactions and transport due to wall reflection, respectively, equation (4) consists of six partial differential equations; one for the transport of each of the six independent Reynolds stresses. The production term (P_{ij}) diffusion (Λ_{ij}), dissipation (ε_{ij}), transport due to turbulent pressure ($\int_{ij}$) and the modelling of the wall reflection (Π_{ij}^{w}) are refereed to (Launder, 1989).

2.2 Flow boundary conditions

Four boundary conditions are considered in accordance with the geometric arrangement of the problem as shown in Figure 1(b); these are:

2.2.1 Solid wall. No slip condition is assumed at the solid wall and the boundary condition for the velocity at the solid wall is therefore:

$$U_i = 0$$

2.2.2 Generalized wall functions for normal and shear turbulent stresses for the RSTM model. When the flow is very near the wall it undergoes a rapid change in direction, the wall-functions approach is not successful in reproducing the details of the flow. Consequently, the turbulent stresses and fluxes at the near wall grid points are calculated directly from their transport equations. In this case, the near-wall region

lying between the wall and the near-wall computational node at x_p can be represented by two layers: the fully viscous sublayer, defined by $Re_v = x_v\sqrt{k_v}/v \cong 20$, and a fully turbulent layer. The wall shear stress near the wall is employed, i.e. $\overline{vw}|_{z_v} = \tau_w/\rho$, which serves as the boundary condition for the $\overline{vw}$ transport equation.

In relation to normal stresses, the turbulence energy must decrease quadratically towards a value of zero at the wall (Benocci, 1991) therefore a zero-gradient condition for the normal stresses is physically realistic. This situation is insufficient to ensure an accurate numerical representation of near-wall effects. An improved approach for internal cells is needed in respect of evaluating volume-integrated production and dissipation of normal stresses (these are normally evaluated at cell centres, using linear interpolation, and then multiplied by the cell volume). Considering $\overline{v^2}$ as an example, the volume-integrated production of $\overline{v^2}$ between the wall and the P-node may be approximated by Hogg and Leschziner (1989), i.e:

$$\int_{\Delta r}\int_0^{z_p} P_{22}\,\mathrm{d}\forall \cong \int_{\Delta r}\int_{x_v}^{x_p} -2\overline{vw}\frac{\partial V}{\partial x}\,\mathrm{d}\forall = 2\tau_w\left(\frac{V_p - V_v}{x_p - x_v}\right)x_p\Delta r \tag{5}$$

where V_p and V_v follow from the log-law. No contribution arises from the viscous sublayer since $\overline{vw} = 0$ in this layer. An analogous integration of the dissipation rate with the assumptions:

$$\varepsilon = \frac{2vk_v}{x_v^2} 0 \le x \le x_v$$

$$\varepsilon = \frac{C_\mu^{3/4}k_p^{3/2}}{kx_v} x_v \le x < x_p$$

leads to:

$$\int_{\Delta r}\int_0^{x_p} \varepsilon\,\mathrm{d}\forall \cong \left[\frac{2vk_p}{x_v} + \frac{C_\mu^{3/4}k_p^{3/2}}{k}\ln\left(\frac{x_p}{x_v}\right)\right]\triangle r \tag{6}$$

an analogous treatment is applied to $\overline{v^2}$, while the production of $\overline{w^2}$ in the viscous and turbulent near wall layers region is zero (Versteeg and Malalasekera, 1995).

The values resulting from equations (5) to (6) are added, respectively, to the volume-integrated generation and dissipation computed for the upper half of the near-wall volume.

It should be noted that for the wall-law approach, the near-wall dissipation (ε_p) is not determined from its differential equation applied to the near-wall cell surrounding the node. Instead, and in accordance with the log law, this value is obtained via the length scale from $\varepsilon_p = C_\mu^{3/4}k_p^{3/2}/kz_p$, which serves as the boundary conditions for inner cells.

2.2.3 Inlet conditions. The boundary conditions for temperature and mass flow rate need to be introduced at nozzle inlet:

$$T = \text{specified}\,(300\,\text{K})\,\text{and}\,\dot{m} = \text{specified}\,(0.0084\,\text{kg/s})$$

The mass flow rate of the annular conical nozzles corresponding to the different configurations is kept the same.

Similarly, the mass flow rate of the pipe is kept the same as the annular nozzles. It should be noted that the pipe length is extended to secure the fully developed turbulent flow in the pipe before emerging from the pipe exit and impinging on to the cavity.

The values of k and ε are not known at the inlet, but can be determined from turbulent kinetic energy, i.e.:

$$k = \lambda \bar{u}^2 \tag{7}$$

where $\bar{u}$ is the average inlet velocity and λ is a percentage.

The dissipation is calculated from: $\varepsilon = C_\mu k^{3/2}/aD$, where D is the diameter. The values $\lambda = 0.03$ and $a = 0.005$ are commonly used and may vary slightly in the literature (Elkaim *et al.*, 1992).

2.2.4 Outlet. The flow is considered to be extended over a long domain; therefore, the boundary condition (outflow boundaries – Figure 1(b)) for any variable ϕ is:

$$\frac{\partial \phi}{\partial x_i} = 0 \tag{8}$$

where x_i is the normal direction at outlet.

2.2.5 Symmetry axis. At the symmetry axis, the radial derivative of the variables is set to zero, i.e.:

$$\frac{\partial \phi}{\partial r} = 0 \tag{9}$$

except:

$$V = \overline{vw} = \overline{vh} = \overline{wh} = 0$$

2.2.6 Solid wall (flat plate surface): uniform heat flux boundary. A uniform heat flux boundary is considered at the flat plate surface. The magnitude of the heat flux is set 1 W/m^2.

2.3 Gas properties

The equation of state is used for air and the properties employed are given in Table II.

3. Entropy analysis

The non-equilibrium phenomenon in a flow system causes a continuous generation of entropy in the flow field. The heat flux is driven by the temperature gradient and the flux of momentum is driven by the velocity gradient. The point-size control volume formulation of the second law gives (Bejan, 1995):

Property		Air
Density	ρ (kg/m^3)	p/RT
Thermal conductivity	K (W/mK)	0.0242
Specific heat capacity	c_p (J/kgK)	1006.43
Viscosity	v (kg/m s)	1.7894×10^{-5}

Table II.
Air properties used in the simulation

$$S'''_{\text{gen}} = \rho \frac{Ds}{Dt} + \frac{\partial}{\partial x_i}\left(\frac{q_i}{T}\right) \geq 0$$

using the energy equation and the identity:

$$\frac{De}{Dt} = T\frac{Ds}{Dt} + \frac{P}{\rho^2}\frac{D\rho}{Dt}$$

the local entropy generation yields:

$$S'''_{\text{gen}} = \frac{K_{\text{eff}}}{T^2}\left(\frac{\partial T_i}{\partial x_i}\right)^2 + \frac{\mu_{\text{eff}}}{T}\Phi \geq 0$$

In two-dimensional polar coordinates:

$$\begin{aligned} S'''_{\text{gen}} = {} & \frac{K_{\text{eff}}}{T^2}\left[\left(\frac{\partial T}{\partial r}\right)^2 + \left(\frac{\partial T}{\partial z}\right)^2\right] \\ & + \frac{\mu_{\text{eff}}}{T}\left[2\left[\left(\frac{\partial V}{\partial r}\right)^2 + \left(\frac{V}{r}\right)^2 + \left(\frac{\partial W}{\partial z}\right)^2\right] + \left(\frac{\partial V}{\partial z} + \frac{\partial W}{\partial r}\right)^2\right] \end{aligned} \tag{10}$$

The first term on the right-hand side of equation (10) is the contribution due to finite heat transfer over finite temperature gradients, and the second term is the local volumetric entropy generation due to fluid friction. As it was stated in the previous study (Drost and White, 1991) that equation (10) is valid for both laminar and turbulent flow; where the effective thermal conductivity is the sum of the molecular thermal conductivity and the eddy thermal conductivity, and the effective viscosity is the sum of the molecular viscosity and the eddy diffusivity. In turbulent flow, therefore, the local volumetric entropy generation depends upon the local spatial gradients of temperature, velocity, conductivity and viscosity. In this case, the conductivity and the viscosity may be written as:

$$K = K_{\text{eff}} = K_{\text{l}} + K_{\text{t}} \qquad \mu = \mu_{\text{eff}} = \mu_{\text{l}} + \mu_{\text{t}}$$

The local quantities of K_{eff} and μ_{eff} are computed for all the turbulence models used in the present study and the associated local volumetric entropy generation is determined.

S'''^{*}_{gen} can be written in non-dimensional form. In this case, the temperature is non-dimensionalized by dividing the jet temperature (T_j) at nozzle exit, spatial length is divided by the annular nozzle equivalent exit diameter ($D = \sqrt{4A/\pi}$, where A is the annular nozzle exit area) and the velocities are divided by the average axial velocity at nozzle exit (V_j). The resulting non-dimensional entropy generation per unit volume becomes:

$$S'''^{*}_{\text{gen}} = \frac{S'''_{\text{gen}} D^2}{K} = \sigma^2(\nabla T^*)^2 + Pr\,E\sigma(\Phi^*) \tag{11}$$

where $\sigma = (T_j/T)$ (T_j is the gas temperature at annular nozzle exit), Pr is the Prandtl number ($Pr = \mu C_{\text{p}}/K$), and E is the Eckert number ($E = V_i^2/(C_{\text{p}}T_j)$).

The volumetric averaged dimensionless entropy generation can be written as:

$$\dot{S}^{*}_{\text{gen}} = \int_{\forall} \frac{S'''_{\text{gen}} D^2}{K} \, \mathrm{d}\theta \, \mathrm{d}z r \, \mathrm{d}r \tag{12}$$

4. Numerical method and simulation

A control volume approach is employed when discretizing the governing equations. The discretization procedure is given in Patankar (1980) The problem of determining the pressure and satisfying continuity may be overcome by adjusting the pressure field so as to satisfy continuity. A staggered grid arrangement is used in which the velocities are stored at a location midway between the grid points, i.e. on the control volume faces. All other variables including pressure are calculated at the grid points. This arrangement gives a convenient way of handling the pressure linkages through the continuity equation and is known as semi-implicit method for pressure-linked equations (SIMPLE) algorithm. The details of this algorithm is given in Patankar (1980).

The computer program used for the present simulation can handle a non-uniform grid spacing. In each direction, fine grid spacing near the gas jet impinging point and the cavity is allocated while gradually increased spacing for locations away from the cavity is considered. The number of grid planes used normal to the x and r directions are 220 and 272, respectively, for the pipe and the conical annular nozzle (Figure 1(b)). The grid independence tests were conducted and it is observed that the grid selected results in the grid independent solution.

Nine variables are computed at all grid points; these are: two velocity components, local pressure, five turbulence quantities and the temperature.

5. Results and discussions

Entropy generation due to flow emerging from an annular conical nozzle and impinging onto a flat plate is considered. The influence of annular nozzle outer angle on the entropy generation rate is examined. Since, the flow field is turbulent, RSTM is employed to account for the turbulence.

Figure 2 shows contours of non-dimensional volumetric entropy generation rate due to fluid friction for four outer angles of annular nozzles. Entropy generation rate is high in the region of nozzle existing and in the vicinity of the plate surface. Since, the nozzle exit velocity profile is non-symmetric due to annular flow, in which case, the rate of fluid strain changes across the nozzle exit vicinity. This in turn results in significant viscous dissipation in this region. Entropy generation rate increases in the region of stagnation due kinetic energy loss. Once the pressure builds up in this region, radial flow is generated along the plate vicinity towards the outlet boundary. This situation results in viscous dissipation in this region, which is more pronounced in the region where flow acceleration is high, i.e. next to stagnation region. Streamline curvature of the impinging jet enhances the frictional losses in the radial direction, since radial momentum dominates the axial momentum in this region. In this case, rate of fluid strain in the region next to the plate surface increases due to increased radial momentum of the jet. The influence of the nozzle outer angle on entropy generation rate becomes high in the region of nozzle exit and stagnation region. Increasing nozzle outer angle modifies the radial distribution of the jet velocity at nozzle exit. In this case,

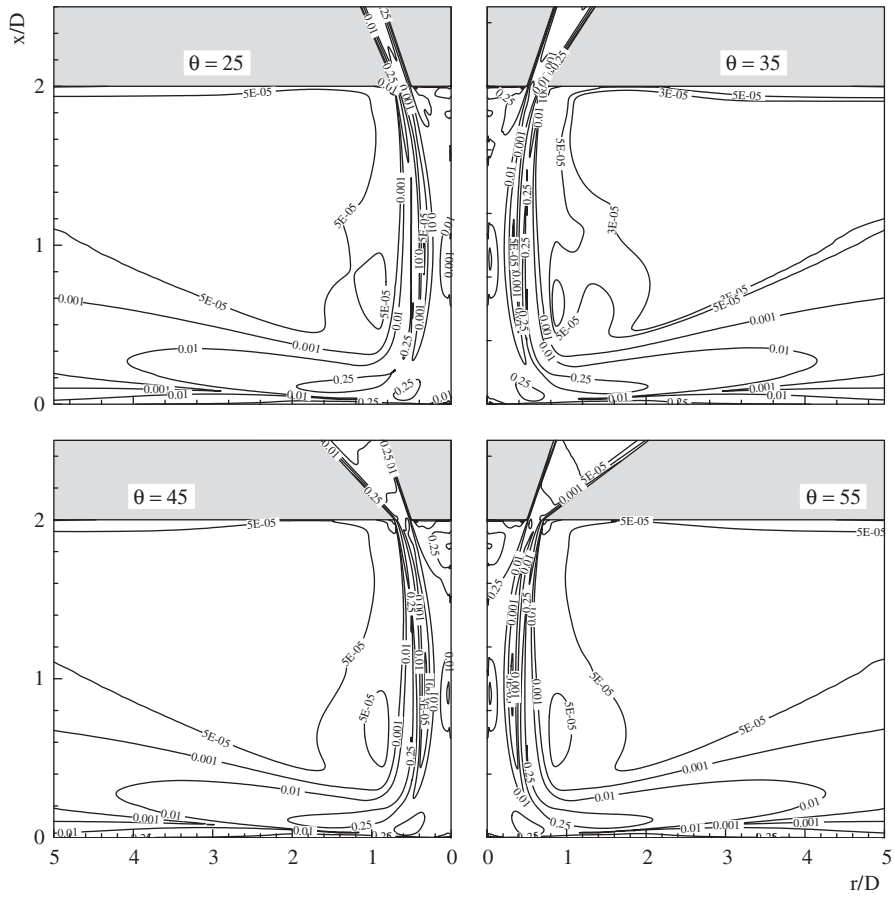

Figure 2.
Entropy generation contours due to friction in the region close to the annular nozzle exit for different nozzle outer angles

increasing nozzle outer angle enhances rate of fluid strain in the region of nozzle exit and in the stagnation region. Consequently, volumetric entropy generation rate increases with increasing nozzle outer angle.

Figure 3 shows contours of volumetric entropy generation rate due to heat transfer for different nozzle outer angles. Volumetric entropy generation rate does not follow exactly to its counter part corresponding to fluid friction, particularly in the region of the nozzle exit. This is mainly because of the heat generation rate due to fluid friction and temperature gradient in the nozzle exit. In this case, heat generated due to fluid friction is transferred to downstream of the jet through expansion of the jet. This, in turn, results in negligibly small temperature gradient in this region. Since, the volumetric entropy generation rate depends on the temperature gradient, which can be considered as flux, and temperature, which can be considered as force, entropy generation rate remains low due to small flux and force terms in this region. Moreover, in the region of the flat plate surface, where flow velocity becomes less, temperature increase becomes more due to thermodynamic pressure (stagnation pressure) as well as

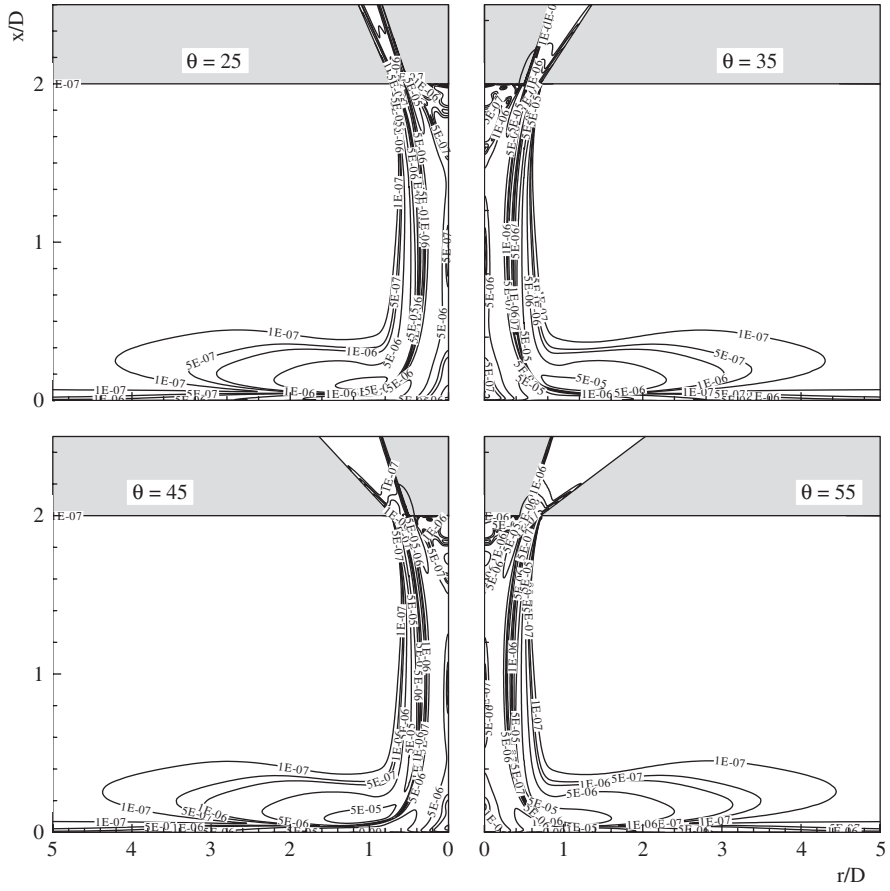

Figure 3.
Entropy generation contours due to heat transfer in the region close to the annular nozzle exit for different nozzle outer angles

high-heat transfer rates. Consequently, force and flux term increase, which in turn enhances entropy generation rate in this region. This argument is also true for the region where radial expansion takes place close to the plate surface. In this case, relatively heated gas in the stagnation region expands radially towards the outlet boundary resulting in notable temperature gradient. This situation enhances entropy generation rate.

Figure 4 shows volumetric entropy generation along the axial direction at different radial locations and for different nozzle cone angles. Entropy generation due to flow emerging from pipe exit and impinging onto a flat plate is also included for comparison reason. Volumetric entropy generation rate is high at the nozzle exit and at the symmetry axis where $r/D = 0$, particularly due to fluid friction. However, in all cases, volumetric entropy generation rate is high in the vicinity of the flat plate due to high rate of fluid strain and temperature gradient because of stagnation heating. Volumetric entropy generation rate is higher due to fluid friction than due to heat transfer. This is mainly because of the jet temperature at nozzle exit which is kept at the same as the ambient temperature. Consequently, contribution of temperature rise and temperature

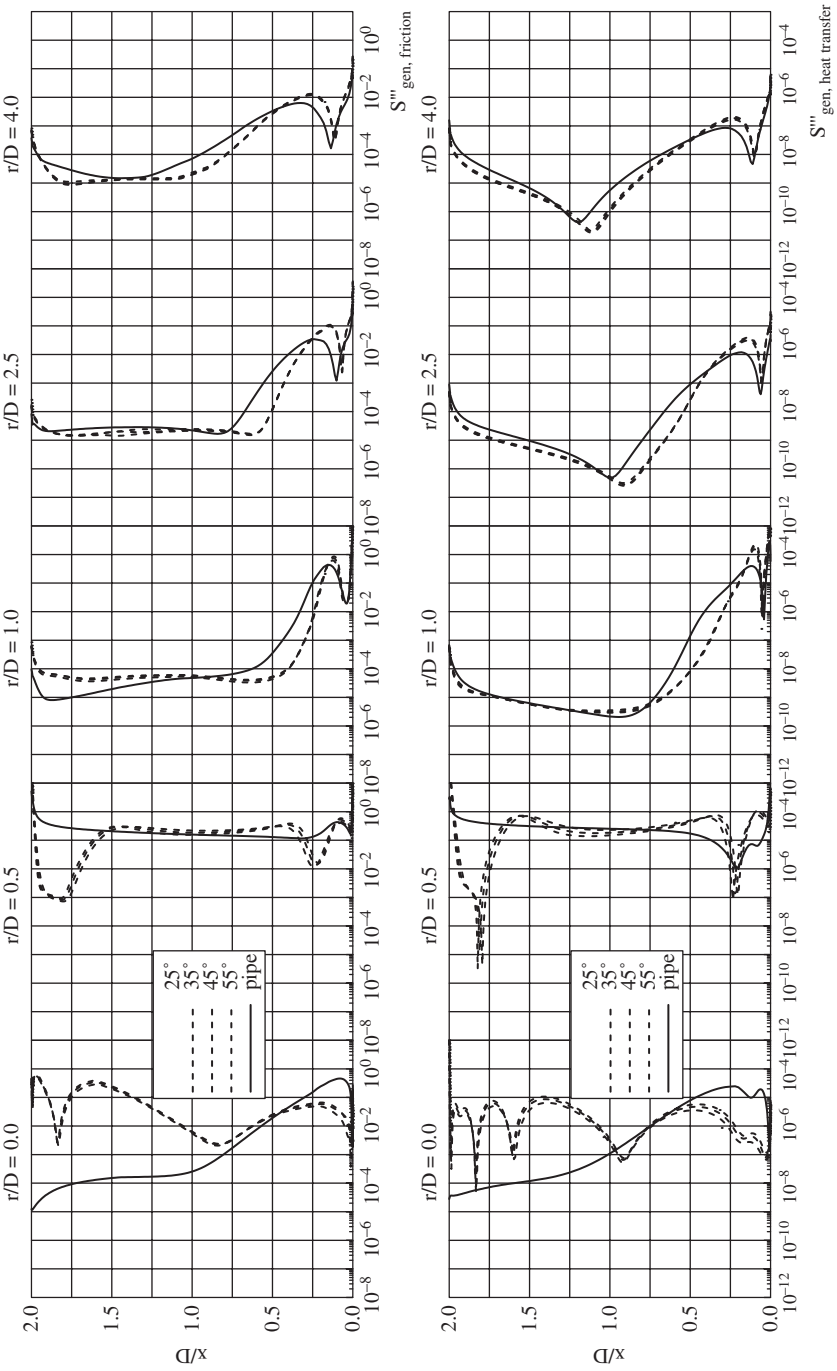

Figure 4.
Volumetric entropy generation rate for annular nozzles and pipe at various r/D locations and different outer angles

gradient on the entropy generation is due to heat generated during fluid friction and thermodynamic pressure rise because of the stagnation point flow. When comparing volumetric entropy generation rates due to flow exiting the pipe and annular nozzle, they behave similarly along the axial direction, except along the symmetry axis where $r/D = 0$. In this case, annular nozzle generates high rate of entropy generation. This is due to complex flow structure generated in the jet emerging from the nozzle, i.e. rate of fluid strain increases at nozzle exit resulting in high rate of entropy generation.

Figure 5 shows total entropy generation rate due to heat transfer ad fluid friction with different nozzle outer angle as well as pipe. Entropy generation due to heat transfer and fluid friction is less for flow emerging from the pipe exit. This can be explained in terms of rate of fluid strain developed in the flow field, which is less for the case of pipe. Increasing nozzle cone angle enhances entropy generation due to both fluid friction and heat transfer effects. This indicates that increasing nozzle outer cone angle increases the kinetic energy dissipation in the fluid. It should be noted that increases in temperature in the flow system is because of heat generated across the shear layers in the fluid. This is the indication of higher rate of entropy generation due to fluid friction than that of heat transfer. Consequently, complex-flow structure enhances the kinetic energy loss in the flow system without significantly increasing temperature.

6. Conclusions

Entropy generation in the flow system due to jet emerging from an annular nozzle and impinging onto a flat plate is examined. The annular nozzle outer cone angle is varied in the simulations in order to investigate the effect of nozzle geometry on the entropy generation. A jet emerging from a pipe and impinging onto a flat plate is also simulated for comparison reason. It is found that volumetric entropy generation rate increases at nozzle exit due to velocity distribution of flow emerging from the nozzle and complex flow structure generated in the vicinity of the nozzle exit. Entropy generation rate

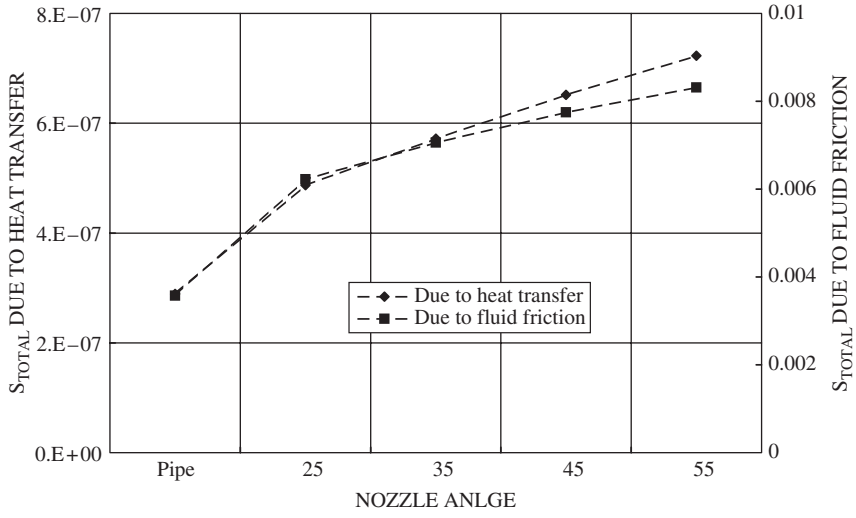

Figure 5.
Total entropy generation rate due to fluid friction and heat transfer

increases in the region of flat plate surface due to radial jet development from the stagnation zone. Volumetric entropy generation rate is higher due to fluid friction than its counterpart corresponding to heat transfer. This is mainly because of the kinetic energy loss which is high in the flow system and heat generated by the shear flow, which is transferred to down stream by jet expansion. This in turn lowers the temperature gradient and temperature rise in the fluid, particularly in the upstream flow. Increasing nozzle outer angle enhances kinetic energy dissipation; consequently, nozzle geometry has significant effect on entropy generation rate.

References

Bejan, A. (1982), "Second-law analysis in heat transfer and thermal design", *Advances in Heat Transfer*, Vol. 15, pp. 1-58.

Bejan, A. (1995), *Entropy Generation Minimization*, 1st ed., CRC Press, New York, NY.

Benocci, C. (1991), *Introduction to the Modeling of Turbulence*, 1991-02, Von Karman Institute for Fluid Dynamics, Sint-Genesius-Rode, March.

Carrington, C.G. and Sun, Z.F. (1992), "Second law analysis of combined heat and mass transfer in internal flow and external flows", *International Journal of Heat and Fluid Flow*, Vol. 13 No. 1, pp. 65-70.

Colucci, D.W. and Viskanta, R. (1996), "Effect of nozzle geometry on local convective heat transfer to a confined impinging air jet", *Experimental Thermal and Fluid Science*, Vol. 13 No. 1, pp. 71-80.

Dano, B.P.E. (2005), "Flow characteristics and heat transfer performances of a semi-confined impinging array of jets: effect of nozzle geometry", *International Journal of Heat and Mass Transfer*, Vol. 48, pp. 691-701.

Drost, M.K. and White, M.O. (1991), "Numerical predictions of local entropy generation in an impinging jet", *Journal of Heat Transfer*, Vol. 113, pp. 823-9.

Elkaim, D., Reggio, M. and Camarero, R. (1992), "Simulating two-dimensional turbulent flow by using the k-e model and the vorticity-stream function formulation", *International Journal for Numerical methods in Fluids*, Vol. 14, pp. 961-80.

Hiroshi, M. and Akira, Y. (1989), "Heat transfer by the annular impinging jet", *Experimental Heat Transfer*, Vol. 2, pp. 1-12.

Hogg, S. and Leschziner, M.A. (1989), "Second-moment-closure calculation of strongly swirling confined flow with large density gradients", *International Journal of Heat and Fluid Flow*, Vol. 10 No. 1, pp. 16-27.

Huang, L. and El-Genk, M.S. (1994), "Heat transfer of an impinging jet on a flat surface", *International Journal of Heat and Mass Transfer*, Vol. 37 No. 13, pp. 1915-23.

Launder, B.E. (1989), "Second-moment closure and its use in modelling turbulent industrial flows", *International Journal for Numerical Methods in Fluids*, Vol. 9, pp. 963-85.

Lee, D., Greif, R., Lee, S.J. and Lee, J.H. (1995), "Heat transfer from a flat plate to a fully developed axisymmetric impinging jet", *ASME Journal of Heat Transfer*, Vol. 117, pp. 772-6.

Lytle, D. and Webb, B.W. (1994), "Air jet impingement heat transfer at low nozzle-plate spacings", *International Journal of Heat and Mass Transfer*, Vol. 37 No. 12, pp. 1687-97.

Mahmud, S. and Eraser, R.A. (2003), "The second law analysis in fundamental convective heat transfer problems", *International Journal of Thermal Sciences*, Vol. 42, pp. 177-86.

Mohanty, A.K. and Tawfek, A.A. (1993), "Heat transfer due to a round jet impinging normal to a flat surface", *International Journal of Heat and Mass Transfer*, Vol. 36 No. 6, pp. 1639-47.

Mukherjee, P., Biswas, G. and Nag, P.K. (1987), "Second-law analysis of heat transfer in swirling flow through a cylindrical duct", *ASME Journal of Heat Transfer*, Vol. 109, pp. 308-13.

Patankar, S.V. (1980), *Numerical Heat Transfer*, McGraw-Hill, New York, NY.

Shuja, S.Z., Yilbas, B.S. and Budair, M.O. (2005), "Influence of conical and annular nozzle geometric configurations on flow and heat transfer characteristics due to flow impingement onto a flat plate", *Numerical Heat Transfer, Part A*, Vol. 48, pp. 917-39.

Versteeg, H.K. and Malalasekera, W. (1995), *An Introduction to Computational Fluid Dynamics. The Finite Volume Method*, Longman Scientific and Technical, Harlow.

Yang, G., Choi, M. and Lee, J.S. (1999), "An experimental study of slot jet impingement cooling on concave surface: effects of nozzle configuration and curvature", *International Journal of Heat and Mass Transfer*, Vol. 42 No. 12, pp. 2199-209.

Yilbas, B.S., Shuja, S.Z. and Budair, M.O. (1999), "Second law analysis of a swirling flow in a circular duct with restriction", *International Journal of Heat and Mass Transfer*, Vol. 42, pp. 4027-41.

Corresponding author
B.S. Yilbas can be contacted at: bsyilbas@kfupm.edu.sa